In 'The Centriole' (ed. V. Kalnins) Acad. Press (1990)

(1)

THE 'IRIS DIAPHRAGM'-PRINCIPLE OF CENTRIOLE AND BASAL BODY FORMATION.

Guenter Albrecht-Buehler

Department of Cellular, Molecular and Structural Biology

Northwestern University Medical School

303 E. Chicago Ave.

Chicago, IL 60611

Tel.: (312) 908-4261

SUMMARY

The paper suggests that the formation and the structure of the microtubular skeleton of centrioles and basal bodies can be derived from the following simple geometric principle.

A closed ring of 9 microtubular initiation sites defines :

a.) a template for the densest packing of 18 additional microtubular initiation sites; and

b.) the shape of 9 rigid arms. Upon swivelling of each arm around a point which is located 4 initiation sites away on the initial ring the array unfolds in a manner similar to the opening of an iris-diaphragm.

As a consequence, the curved shape of the microtubular triplet blades arises together with the clockwise rotational sense of the slanted blades of the centriole or basal body. The final diameter of the centriole (basal body) self-adjusts. Furthermore, the pitch of the triplet blades, the taper of centrioles and basal bodies and the change of slant of the blades towards the distal end can be derived. In addition, a method of replication of pro-centrioles (pro-basal bodies) is implied.

The hypothesis is supported by the fitting of electron microscopical cross-sections of centrioles of 3T3 cells to the geometric shapes predicted by the model.

INTRODUCTION

More than thirty years have passed since it was learned that centrioles and basal bodies share the same spectacular ultrastructural organization (Burgos and Fawcett, 1955; Porter, 1956). It was also soon discovered that they belong to Nature's most conserved cellular structures. Taken from different organisms and cell types, they may differ as to the presence and morphology of rootlets, alar sheets, basal feet, basal plates, cartwheels etc., but with very few exceptions they all share the 'skeleton'-structure of microtubules that is shown schematically in Fig. 1. Exceptional centriole structures were found only in a number of sperm cells (Phillips, 1966; Bacetti et al., 1973; Phillips, 1974; Shay, 1974; Goldstein, 1977; Prensier et al., 1980).

The majority of cases which were studied during the past 30 years by electron microscopy (e.g. Brinkley and Stubblefield, 1970) show centrioles or basal bodies as cylindrical structures of 0.2 - 0.3 μm diameter and 0.4 - 0.7 μm length which taper towards one end at an angle of 3 -7 ^{o} (see Fig. 1). The narrower end is called 'distal', the wider end 'proximal'. The mantle of the cylinder is divided laterally by nine identical and equally spaced microtubular arrays, called 'blades'. Each such array consists of three microtubules which form an angle ('pitch') of 10 -15^{o} with respect to the centriole axis (Anderson, 1972). The cross-section of each blade shows the three microtubules lined up side by side and forming an arc which points its convex face away from the centriole axis. Each blade contains one complete microtubule (The A-tubule with a circular cross-section) and two incomplete microtubules (B-, and C-tubules with c-shaped cross-sections). The nine arc-shaped triplet blades slant outward from the perimeter of the centriole in a clockwise rotation if viewed from the distal end. In cross-section, the angle between the blades and the perimeter of the centriole decreases towards the distal end in mature centrioles (cf. Fig. 2 c and d). For the sake of simplicity the exact cross-section and the changing slant of the

triplet blades were omitted from Figure 1, but will be used further below to support the model presented here.

Condensing the above description into a list of keywords, one may say that the microtubular skeleton of centrioles and basal bodies is characterized by the following features.

1. cylindrical structure

2. taper of the cylinder

3. 9-fold rotational symmetry

4. composition of the blades from one complete and two incomplete microtubules

5. convex shape of the blades

6. pitch of the blades

7. clockwise rotational slant of the blades

8. the increasingly tangential slant of the blades towards the distal end.

The formation and replication of centrioles and basal bodies is still a mystery. The literature, however, provides many consistent observations such as the following which may serve as clues.

9. Fibrous coils of about 1200 A diameter have frequently been seen to precede centriole and basal body formation (Kalnins and Porter, 1969; Anderson and Brenner, 1971; Manton et al., 1970; Perkins, 1970; Pickett-Heaps, 1973).

10. The inner and outer diameter grows during maturation of centrioles and basal bodies (cf. Fig. 2a-d).

11. The initially radial slant of the blades turn more tangential as centrioles and basal bodies mature (Brinkley and Stubblefield, 1970; Dippell, 1968; Grimes, 1973; Moser and Kreitner, 1970; Turner, 1968; Alvey, 1985; Tamm and Tamm, 1980; cf. Fig. 2b and d).

12. The slant of the blades is more tangential at the distal than at the proximal end which may have the following reason. In many cases the mature centriole becomes the basal body of a primary cilium (Sorokin, 1962; Wheatley, 1966; Albrecht-Buehler and Bushnell, 1980; see Fig. 2e and 3g)). Consequently, the slant of the blades at the distal end of the centriole must be almost tangential (see Fig. 2e, second panel from above) in order to accomodate the tangential orientation of the ciliary doublets (Fig. 2e upper panel).

13. Connecting fibers appear to span the distance between adjacent blades in centrioles and basal bodies (Allen, 1969; Anderson and Brenner, 1971; Dippell, 1968; Gibbons and Grimstone, 1960; Turner, 1968; and cf. Fig, 2d),

14. The A-tubule of the forming blades is the first of the three blade microtubules to grow in length followed by the B- and C-tubule (Anderson and Brenner, 1971; Dippell, 1968; Grimes, 1973; Kalnins and Porter, 1969)

On the other hand, some well-established observations about centriole and basal body formation may be ignored by the model, because they are not generally true. For example, it is well demonstrated that centrioles and basal bodies usually arise from existing centrioles or basal bodies. However, they can also form *de novo* (Turner, 1968; Manton et al. ,1970; Moser and Kreitner, 1970; Perkins, 1970; Pickett-Heaps, 1973;).

Another such well-established observation is the usual locatior of the newly forming so-called pro-centrioles or pro-basal bodies (Gall, 1961) facing the wall of the mother-centriole or mother-basal body (see Fig. 3a-c). Nevertheless, there are exceptions to this rule as well. In several cases the new centrioles or basal bodies do not form at right angles but rather end-to-end of an existing one (Berlin and Bowen, 1964; Moser and Kreitner, 1970; Perkins, 1970) or in a 'cloud' of up to 10 precursors during ciliogenesis (Kalnins and Porter 1969;Anderson and Brenner, 1971; Komatsu and Fujita, 1978).

Therefore, we may regard the usual method of centriole and basal body replication orthogonally to the axis of an existing mother as incidental to the mechanism of replication. Nevertheless, as published earlier, we consider the orthogonal orientation of the two centrioles as essential for their function as cellular devices to locate signal sources around migrating cells (Albrecht-Buehler and Bushnell, 1979; Albrecht-Buehler, 1981).

The features 1 through 14 of centrioles and basal bodies seem sufficiently informative to allow one to reduce the observations to a very simple geometric principle that explains the above list of features in a qualitative and quantitative sense. The present article introduces this principle.

RESULTS

(Note: With the exception of Fig. 2c, e and 6k all cross-sectional views of centrioles are seen from the distal towards the proximal end)

1. Bud formation.

We assume that the formation of a centriole (basal body) begins with a ring of nine microtubular precursors spaced in such a way that nine microtubules could be accomodated in a wall-to-wall configuration (Fig. 4a). This structure will be called the bud. Based on a microtubular radius of t=120 A, the bud diameter D_b is

$$\{1\}\quad D_b = 2t\,[\{1/\sin(20^o)\}+1] = 940\ A$$

The bud is likely to resemble a fibrous coil because the connections between the different precursors are likely to involve fibrous polymers. As mentioned in the introduction, fibrous coils of diameters in the range of 1000 A have been observed to precede centriole and basal body formation. The ring structure of nine wall-to-wall microtubules has been observed in connection with centrioles, too. The mature centriole of the *Ascaris* sperm appears in cross section identical to Fig. 4a (Goldstein 1977). Therefore, from the point of view of this model, the *Ascaris* sperm appears as the 'minimal centriole structure'.

In order to generate the more complex structure of common centrioles, the bud has to add 18 more mictrotubular precursors. We assume that the additional precursors are packed together in the densest possible way (See Fig. 4 b and c). In consequence, the diameter of the bud grows to about 1400 A. As shown by the cross-hatched microtubular precursors in Fig. 4, the densest packing automatically generates a curved arrangement of microtubular cross-sections similar to the known cross-section of centriolar blades (cf. Fig. 2).

2. Formation of swivel arms.

A major postulate of the model is the formation of fibrous arms which extend around the perimeter of the bud along 4 microtubular diameters. One of the nine arms is drawn in Fig. 4 as a polygon of 4 segments that stretch from center to center of 5 consecutive microtubular precursors. The number 4 of the segments covered by each arm is essential for the model. If one changes it to 3 or 5 the resulting structures are markedly different from actual centrioles and basal bodies.

The model assumes that each of the nine arms is rigidly connected to the 3 specific microtubular precursors which are cross-hatched in Fig. 4c. Thus it divides the bud into 9 identical structures which will be called 'swivel arms'. One of them is shown in Fig. 4d. The free end of each arm is assumed to be able to swivel around a 'hinge' (marked '*' in Fig. 4d) in a fashion shown in Fig. 4e. Please note, that each hinge coincides with the center of one of the microtubular precursors of the bud. The main idea of the 'iris diaphragm' principle of centriole (and basal body) formation is expressed in the following 2 postulates.

a. The 9 hinges remain fixed in their relative position by an assumed special structure.

b. The 9 arms remain rigid while swivelling around their hinges (cf. Fig. 4 e).

We will show that the known microtubular skeleton results from the above postulates in surprisingly accurate detail.

3. Blade curvature.

If we assume that centriolar microtubules and basal body microtubules are composed of 13 protofilaments like ordinary microtubules, important contraints on the shape of the future blades result. For example, the B-tubule must share 2 of the protofilaments with the A-tubule (see Fig. 5a). Since the number 13 of protofilaments is odd the C-tubules cannot be attached along the straight line that connects the centers of A and B (Fig. 5a). It must turn aside in order to share the protofilaments labelled 1 and 1' in Fig. 5a. Consequently the resulting triplet is curved similar to the shape of blades of actual centrioles and basal bodies. The blade curvature can be described by the the angle cu = τ (See Fig. 5a) which measures how much the center C of the C-tubules is shifted away from the mid-line connecting the A- and B-tubules.

There is a second possibility to attach the C-tubule by sharing the protofilaments labelled 2 and 2' in Fig. 5a. In this case the blade curvature cu = 3τ. The two possibilities gives rise to different bud structures. If the blade curvature cu = 3τ the bud structure of Fig. 5b arises; if it is cu = τ than the blades slant out more radially as shown in Fig. 5c. For the following illustrations the blade curvature is assumed to be cu = 3τ.

In addition to these two possibilities the blade curvatures could assume values of cu = $-\tau$ and cu = -3τ which correspond to the mirror images of the blade structures described above. Ultimately, these blade curvatures would require to mirror image every other structure of the bud and, in consequence, the entire centriole structure. However, mirror image-centrioles have never been observed. On the contrary, sections through large fields of basal bodies in the surface of ciliated cells and serial sections of centrioles which formed end-to-end (Berlin and Bowen, 1964; Moser and Kreitner, 1970; Perkins, 1970) showed unambiguously that all centrioles and basal bodies have the same handedness. Therefore, we ignore in the

following the possibility that the model is compatible with normal and mirror image centrioles. Instead, we describe the formation of only one of the two stereo-isomers, and return to the question of mirror image-structures in the Discussion.

4. Unfolding of the bud.

As indicated in Fig. 4e each rigid arm can rotate in only one direction around its hinge, namely clockwise. Counter-clockwise rotation would result in a compression of the microtubular precursors beyond their densest packing which is not possible. In contrast, the counter-clockwise rotation of the arms opens up the array similar to the opening of the individual segments of an iris-diaphragm. Figure 6a-j shows the various stages of the unfolding of the bud. Consistent with experimental data (Anderson and Brenner, 1971; Tamm and Tamm, 1980) the outer diameter and inner lumen of the procentriole increase while the blades slant out in a rather radial direction (Fig. 6a-d). Subsequently, the array reaches a maximum diameter at a swivel angle ϕ_{max} (Fig. 6g). Further rotation turns the blades more tangential, while the radius of the array decreases again (Fig. 6h-j). Eventually the process stops when consecutive blades hit each other front-to-end (Fig. 6j). At this stage the slant of the blades is almost tangential.

5. The necessity of connectors between blades.

In addition to programming a computer to simulate the unfolding, we built several mechanical models in order to test it (Fig. 6k). In particular, we hoped to understand how the bud had to be designed in order to prevent entangling of the arms during the unfolding. Besides having to be rigid and curved as shown in the previous Figures, we found that the arms had to fulfil 2 further conditions:

a. Consecutive blades had to be connected by flexible fibers ('connector') whose length corresponded to the maximal distance between adjacent blades (i.e. the distance between blades shown in the configuration of Fig. 6g). Figures 6k and 7 indicate the location of such connectors labelled 'Co'. The mechanical model

demonstrated how the connectors prevented the tangle: If a blade approached the preceding one, it had to stretch the connector behind it, thus pulling up the rear blade. This in turn pulled up the blade 2 places behind it and so forth all around the circle until the pull had reached the blade in front, which now pulled away from the approaching blade and cleared the space. In this way entangling of the arms was impossible, and an even opening of the array guaranteed. Many such connectors must be attached along the entire lengths of the blades in order to be effective.

Consistent with the model, such connectors are regularly seen between the blades of centrioles and basal bodies (Allen, 1969; Anderson and Brenner, 1971; Dippell, 1968; Gibbons and Gromstone, 1960; Turner, 1968). The two lower panels of Fig. 2d show such connectors. Obviously, they exist in at least two different planes along the centriolar axis. In longitudinal sections such as Fig. 3f one can detect a large number of fibers which run 'horizontally' between blades.

b. The arms must not lie in a plane but spiral slightly downwards. Figure 8 shows this requirement in a stereo pair. As shown by the mechanical model, this condition guarantees that the arms cannot touch each other during the swivelling.

6. The axial growth of the blade microtubules.

As is well known from the literature and illustrated in Fig.3, the pro-centrioles and pro-basal bodies grow in length while their diameter increases (see Fig. 3a-f). The first microtubule to grow is the A-tubule followed by the B- and C-tubules (Kalnins and Porter, 1969; Anderson and Brenner, 1971). Despite large statistical samples and careful observations the speed of the growth of the blade microtubules is not yet known (Alvey, 1985).

According to our model, the arms are still in the process of swivelling while the blade microtubules grow in length as shown in Fig. 9. Figure 9 assumes that the blade tubules grow downwards, i.e. the array of arms will eventually become the distal end of the mature centriole or basal body. This assumption is not vital for the validity of

the model, but as pointed out in the next section, it allows a simple explanation for the pitch of the blades, the taper of the entire structure, and perhaps even the swivelling mechanism itself (see Discussion).

7. Pitch, taper and changing slant of the blades towards the distal end.

According to the previous section, the model assumes that the swivelling action occurs at the future distal end of the centriole. Consequently, it is reasonable to assume, that mechanical resistance of the surrounding cytoplasm will cause the blades at the proximal end to lag behind in their rotation. The lag will not correspond to a large difference in swivel angle because the connectors all along the blades can be expected to couple the movement of the blades reasonably well to each other. Nevertheless, a lag of some size must be expected, and it entails a number of important consequences.

For example, if the swivelling at the distal end has reached the state of Fig. 6i, the rotation at the proximal end may still be in the state of Fig. 6f. As a result (see Fig. 10),

a. the blades are pitched by 10-15^{o} as in actual centrioles and basal bodies (Anderson and Brenner 1971)

b. the diameter of the proximal end is larger than the diameter of the distal end (see Fig. 1, 3f and 10),

c. at the proximal end the blades slant out more radially than at the distal end, provided the swivelling angle at the distal end exceeds the angle ϕ_{max} of maximal unfolding. Especially, the slant of the blades at the distal end of basal bodies may become almost completely tangential. This orientation is essential for the function of basal bodies and centrioles as nucleation sites for the axonemes of normal and primary cilia. Since the orientation of the outer doublets of ciliary axonemes is tangential and since it is determined by the orientation of the triplet blades of the

basal bodies, the blades at the distal ends of basal bodies need to be oriented tangential. The model accommodates this requirement very easily.

8. Replication.

The process of replication is outside the scope of this article which is only concerned with the principle of maturation of centrioles and basal bodies. In particular, the model does not need to suggest any specifics of the location of the reproduction because, as mentioned earlier, the location of reproduction is highly variable. Nevertheless, it should at least offer an idea how the starting structure, namely the bud, could be reproduced by the mature structures. According to present knowledge, the pro-centrioles appear about 4 hours after the onset of DNA-replication (Vorobiev and Chentsov, 1982; Alvey, 1985)

At least in principle, the templating of the bud by the mature structure is not very problematic, because the essential geometric feature of the bud, namely the arrangement of the nine microtubular precursors, never changed during the unfolding process. After all, it served as the fixed set of hinges for the different arms. Particularly, during the stages shown in Fig. 6 h-j the configuration of the arms re-establishes the initial ring of 9 microtubular precursor sites (see arrow in Fig. 6h). Therefore, it seems possible, that this reformed ring becomes the template for the new bud structure. Consistent with the above assumption that the swivelling arms are located at the distal end of centrioles and basal bodies we suggest, therefore, that the new bud is formed from a template at the distal end. Of course, the model cannot predict how the new bud is transported to the various observed sites of maturation outside the maternal structure. In particular, basal bodies seem to present a problem for the transport, because their distal end is capped by the basal plate and the ciliary axoneme. Therefore, we may have to postulate that the buds for procentrioles travel through the lumen of the basal body from the distal end to the proximal end where they enter the surrounding cytoplasm.

9. Quantitative aspects of the model.

In order to describe the unfolding of the bud in quantitative terms we define several variables which are introduced in Fig. 11. The Figure shows an arm in its initial position (thin lines) and after it has swivelled by an angle ϕ around its hinge 'S' into a new position (thick lines). The new radii of the centriole are the inner radius (= the radius of the lumen) R_i and the outer radius R_O (Fig. 11b). The slant of the blades is measured by the angle 'bl'(Fig. 11a) which measures the angle between the tangent to the centriole periphery and the connecting lines between the centers of the A- and C-tubules. This angle changes during the unfolding of the bud. In contrast there is a fixed angle between the arm and the connecting line between the centers of the A- and B-tubules which is indicated as 'nbl'. The curvature of the blades was explained in Fig. 5 and is denoted as 'cu'. As noted above, the only values that the blade curvature can assume are $cu=\tau=(360^O/26)$ and $cu=3\tau$. Consistent with equation {1}, the radius of microtubules is denoted as t=120 A. Furthermore, we define

ϕ := the swivel angle of the arm

$\sigma := 360^O/9 = 40^O$ (the angle resulting from the 9-fold symmetry of centrioles).

Using these notations a lengthy, but elementary calculation yields the following relationships between the variables

{2} $R_i = R_{i0}\, H(\phi) - t$

{3} $R_O = [\, e^2 + R_{i0}^2 - 2e\, R_{i0} \cos(\phi+\sigma/4+\delta)\,]^{1/2} + t$

{4} $bl = \alpha+\theta-90^O$

with

{5} $R_{i0} = t / \sin(\sigma/2)$

{6} $H(\phi) = [\, 1 + 4\cos^2(\sigma/4) - 4\cos(\sigma/4)\cos(\phi+\sigma/4)]^{1/2}$

{7} $\delta = \cos^{-1}[(e^2 + c^2 - b^2) / 2ec]$

{8} $e = [\, c^2 + b^2 - 2bc\cos(\alpha)]^{1/2}$

{9} $c = 2\,R_{i0}\cos(\sigma/4)$

{10} $b = 4t\cos(cu/2)\cos(3\tau)$

{11} $\alpha = 90^{o} + \sigma/4 + nbl - (cu/2)$

{12} $\theta = \cos^{-1}[\{c^2 + (R_i+t)^2 - R_{i0}^2\} / 2c\,(R_i+t)]$

Figure 12a shows the the blade angle bl as a function of the swivel angle ϕ for 3 different values of the fixed arm angle nbl with constant curvature of $cu=3\tau=41.53^{o}$. The graph shows that a maximal slant of the blades occurs at a swivel angle of $\phi_{max}=50^{o}$ with a subsequent reduction of the slant until the blades are tangential and hit each other front-to-end (bl=0). This final state of the unfolding is reached at different values of swivel angles ϕ depending on the fixed angle nbl of the arm. For example the blades turn almost tangential at $\phi_{final}= 250^{o}$ for $nbl=70^{o}$. Similar curves are obtained for different values of the blade curvature $cu=\tau=13.8^{o}$ or $cu=3\tau$ and a constant fixed angle of the arm $nbl=70^{o}$ (Fig. 12b).

Fig 12c and d show the inner and outer radii of the unfolding centriole as a function of the swivel angle ϕ for different values of nbl at a constant blade curvature of $cu= 41.53^{o}$ (Fig. 12c) and for different blade curvature at a constant value of the fixed arm angle $nbl=70^{o}$ (Fig. 12d). The graphs show the initial expansion of the radii until the maximum size is reached at a swivel angle of $\phi\approx140^{o}$. At this angle the slant of the blades has already passed its maximum and the blades have returned to approximately the slant they had in the bud structure at $\phi=0^{o}$.

The growth of the inner radius (lumen) and the outer radius are shifted in phase. Due to the change of the blade angles the inner radius reaches its maximum later than the outer radius. Therefore plots of the inner radius as a function of the outer radius yield curved lines (Fig. 12 e,f).

<u>10. Fitting of centriolar cross-sections.</u>

In order to test the accuracy of the model we used electron micrographs of centriolar cross-section of 3T3 cells and tried to match them with computed cross-

sections of centrioles. The match was considered successful if the computer-drawn outlines coincided with the electron micrographs within the thickness of a microtubular wall (≈80 A).

For the fitting procedure, we allowed a certain shrinkage of the Epon sections of up to 25%. In general, the shrinkage was not the same in different directions resulting in centriolar cross-sections that were not exactly circular but slightly elliptical. The difference in shrinkage was measured by an axial distortion factor which expressed the ratio of the two main axes of the resulting ellipse. We selected 45 serial cross-sections and 17 individual sections of 15 centrioles from interphase cells and 8 individual sections from 8 centrioles of mitotic cells in metaphase. The interphase centrioles included several maturing centrioles.

The fit was easily possible in every case. We used the following recursive protocol.

a. Determination of the distortion factor from the ellipticity of the cross-section.

b.Choice of the blade curvature ($cu=\tau$ or $cu=3\tau$)

c. Determination of the inner radius R_i (indep. of fixed blade angle nbl)

d. Using Equ. 2 and 7, determination of swivel angle ϕ

e.Determination of shrinkage from the discrepancy between the computed outer radius R_O and the experimental value.

f. Repetition of steps d-e until the computed outline on a flatbed-plotter coincided with the centriolar outlines on the enlarged (300,000x) micrograph.

As an example, Fig. 13 shows the fitted outlines of the centriolar serial cross-section of column b of Fig.2. It used a shrinkage factor of 22% and an axial distortion factor of 1.05. In all three computations the fixed blade angle was $nbl=70^O$ and the curvature $cu=\tau=13.85^O$. The remaining parameter to be fitted was the swivel angle ϕ. Consistent with the hypothesis that it is larger at the distal end, this particular example yielded $\phi=190^O$ for the distal end (Fig. 13a) and $\phi=140^O$ for the proximal

end (Fig. 13c). The more central section of Fig. 13b yielded also $\phi = 140^{o}$ suggesting that it was located closer to the proximal than to the distal end.

DISCUSSION.

Movement as part of the assembly of a cellular structure.

Considering the large number of geometric characteristics of centrioles that can be derived from the iris diaphragm-principle, it seems legitimate to take it more seriously than a mere mathematical game. Consistent with conventional ideas about the assembly of other cellular structures, the model assumes that the formation of centrioles and basal bodies begins with the assembly of many macromolecular components into a precursor structure (the bud) which uses a template (the arrangements of the nine arms after the unfolding; see Fig. 6h). The macromolecular assembly continues with the growth of the blade microtubules. The new feature of the model is the introduction of a movement (the unfolding of the bud) as a major component of the formation of centrioles. Given today's requirement of specimen fixation and dehydration for electron microscopy, this movement cannot be observed directly. However, nearly every intermediary configuration of the blades that is postulated by the model has been observed at one time or another by workers in the field.

Reduction of the complex centriolar geometry to a small number of mostly known constants.

A further special feature of the model is its reduction of the quite complex geometry of centrioles and basal bodies to only 4 basic numbers:

a. the radius of microtubules (120 A),

b. the rotational symmetry of centrioles (9-fold),

c. the rotational symmetry of microtubules (13-fold), and

d. the number of segments of the initial ring structure covered by the arm (4 segments).

For example, the bud structure results from the microtubular radius and the 9-fold symmetry. The blade curvature is a consequence of the radius and the 13-fold symmetry of the microtubules. The arm structure and location of the hinges follows from the microtubular radius, the 9-fold symmetry and the number 4 of the segments covered by the arm, and so forth.

It may appear that the fixed blade angle nbl is a fifth parameter of the model. However, it is actually a consequence of the packing of microtubular precursors in the bud. In all the fitting procedures and in the illustrations we used nbl=70^{o}=90^{o}-$\sigma/2$. Therefore, the fixed angle is actually a consequence of the 9-fold symmetry of centrioles and basal bodies. In the graphs of Fig. 12 we included larger and smaller angles for reasons of completeness.

The other features of the centriole structure, e.g. pitch of the blades, taper of the centriole and the automatic termination of the maturation process are consequences of the swivelling process itself.

The simplicity of the underlying set of premises of the model is also expressed in equations 1-12. They contain as fundamental parameters only

a. t=120 A (microtubular radius),

b. $\sigma=360^{o}/9=40^{o}$ (expression of the 9-fold symmetry of centrioles),

c. $\tau=(1/2)\ (360^{o}/13)$ (expression of the 13-fold symmetry of microtubules)

d. the occurrence of $\sigma/4$ (expression of the number of segments covered by the arm).

Speculation about possible swivelling mechanisms.

Thus the main assumption of the model is the presence and action of a swivelling mechanism which is expressed in the equations by the swivel angle ϕ. The assumption is compatible with present day knowledge.

As to the generation of the swivelling motion, there are numerous helical polymers in cells that are capable of producing torque by undergoing conformational

changes. One may even think that a eukaryotic analog of the rotary engine of bacterial flagella may turn the swivelling arms. Another way of unfolding the bud could be achieved by the earlier mentioned fibers that we called the 'connectors'. In the Results section we explained their presence by their ability to prevent the entangling of the swivelling arms during unfolding. It is conceivable that they also act as combined 'connectors-expandors', i.e. as rods that elongate by polymerization and thus pry adjacent blades apart while they pull up the other blades further away. However, this possibility seems less attractive because it would require that the 'connector-expandors' shorten again after the array of arms has gone through its maximal diameter. Another, rather intriguing mechanism to generate the swivelling motion may be provided by the simultaneous growth of the blade microtubules themselves. They are pitched and consequently elongate in an oblique direction relative to the axis of the future centriole. Any mechanical resistance in the cytoplasm can be expected to automatically push their base (=arms) in the opposite direction. The resulting torque would turn the arms in precisely the required direction of swivelling (cf. Fig. 9 and 10).

Location of the swivelling mechanism at the distal end.

The model links the pitch of the blades, the taper of the centrioles and basal bodies, and the almost tangential slant of the blades at the distal end together as common consequences of the swivelling mechanism. Consistent with this explanation, we suggested that the arms and the swivelling mechanism were located at the distal end during the maturation process. Of course, the suggestion does not specify how far along the axis the array of arms extends. The model would also be compatible with the presence of several arrays of arms stacked underneath each other along the axis. For example, the fibrous plug seen in Fig. 3f which extends from the distal end along the axis down to about 2/3 of the length of this centriole may be interpreted as an axially extended swivelling machinery.

In order to explain the link between these different geometric features of centrioles and basal bodies we assumed that the elongating blade microtubules were anchored in the distal end while their free ends pointed downward to the proximal end (Fig. 9). The latter assumption is not essential. It would not invalidate the model if the growing blade microtubules were anchored at the proximal end while pushing the distally located swivelling machinery further and further away. In particular, the explanation of Fig. 9 does not intend to predict where the new tubulin dimers are added to the growing microtubules. Nevertheless, the model claims that the swivelling mechanism is located at the distal end. Consequently, the model also claims that it is distinct from the so-called cartwheel structure.

The cartwheel structure is usually located at the proximal end. It is a radial array of fibers connected by a central hub (see arrow in Fig. 2b {3rd panel from the top}) which is disassembled in mammalian centrioles after their maturation. The 2 bottom panels of Fig. 2b show an example of the cartwheel. Since it is reminiscent of the array of arms postulated by our model, it is tempting to consider it as a candidate for the swivelling mechanism. However, this interpretation of the cartwheel would place the swivelling mechanism at the proximal end in contrast to the assumptions of the model. Therefore, we interpret the cartwheel as a bracketing device to prevent the growing blade microtubules from fraying out during the combined movements of growth and unfolding.

<u>The question of mirror-image centrioles and basal bodies.</u>

If it were not for pitch and taper, each centriole and basal body would be identical with its mirror image turned upside down. In principle, taper and pitch need not be linked by the same mechanism. Only the present model suggested that they are. Therefore, it is conceivable that there are four classes of centrioles and/or basal bodies. One class contains the structures similar to Fig. 1 , the other class contains their mirror images. The third class contains structures that look like Fig.1 except

that the pitch of the blades is the opposite, i.e. they lead from the bottom left-hand side to the top right-hand side. The fourth class represents the mirror images of the third class. It is remarkable that three of the four classes have never been observed. Only the structures shown in Fig.1 seem to exist in nature. The model presented here reduces the problem of explaining this remarkable fact. Since it interprets taper and pitch as common consequences of a difference between the swivel angles at the proximal and distal end, it eliminates the classes three and four. It also links the sign of the blade curvature i.e. whether $cu=\tau$ or $cu=-\tau$, with the direction in which the attached arms extend around the initial ring, and consequently it links it with the direction of swivelling: Given the blade curvature, the other two quantities can only assume one particular direction, or else the array cannot unfold. Therefore, one may say that the model reduces the mechanisms that determine the handedness of the centriole and basal body structure to the mechanisms that determine either the sign of the blade curvature or the direction in which the blade microtubules elongate. Either way, the model reduces the fundamental question of the determination of handedness of centrioles and basal bodies to a question about properties of microtubular assembly.

ACKNOWLEDGMENT.

Parts of the work presented here date back as far as 10 years. During this time I was supported by a number of different grants. In its most recent phase the work was supported by grants from the Office of Naval Research (N00014-89-J-1700) and the U.S. Army Resarch Office (26385-LS). A major basis of the work was a large number of electron micrographs of centrioles expertly and patiently produced 8 years ago by Ms. Anne Bushnell. I am very grateful for hers and Ms. Amy Alberts' excellent assistence. Last but not least I should like to thank Martin Zand for his critical reading of the manuscript.

REFERENCES

Albrecht-Buehler, G. and Bushnell, A. (1979) The orientation of centrioles in migrating 3T3 cells. Exp. Cell Res. 120:111-118

Albrecht-Buehler, G. and Bushnell, A. (1980). The ultrastructure of primary cilia in quiescent 3T3 cells. Exp. Cell Res. 126:427-437.

Albrecht-Buehler, G. (1981). Does the geometric design of centrioles imply their function? Cell Motility 1:237-245

Allen, R.D. (1969) The morphogenesis of basal bodies and accessory structures of the cortex of the ciliated protozoan *tetrahymena pyriformis*. J. Cell Biol. 40:716-733

Alvey, P.L. (1985). An investigation of the centriole cycle using 3T3 and CHO cells. J.Cell Sci. 78:147-162.

Anderson, R.G.W. and Brenner, R.M. (1971). The formation of basal bodies (centrioles) in the Rhesus monkey oviduct. J. Cell Biol. 50:10-34

Anderson, R.G.W. (1972). The three-dimensional structure of the basal body from the Rhesus monkey oviduct. J.Cell Biol. 54:246-265

Bacetti, B.,Dallai, R., and Fratello,B. (1973) The spermatozoa of arthropoda. XXII. The 12+0, 14+0 or aflagellate sperm of *Protura*. J.Cell Sci. 13:321-335

Berlin, J.D. and Bowen, C.C. (1964). centrioles in the fungus *albugo candida*. Am. J. Bot. 51:650-652

Brinkley, B.R. and Stubblefield, E. (1970) Ultrastructure and interaction of the kinetochore and centriole in mitosis and meiosis. In Advances in Cell Biology, Vol.1 (ed. Prescott,D.M., Goldstein L. and McConkey E.) p. 119-185

Burgos, M.H. and Fawcett, D.W. (1955) Studies on the fine structure of mammalian testis. I. Differentiation of the spermatids in the cat (*felis domestica*). J. Biophys. Biochem. Cytol. 1:287-300

Dippell, R.V. (1968) The development of basal bodies in *paramecium*. Proc. Natl. Acad. Sci. U.S.A 61:461-468.

Gall, J.G. (1961) Centriole replication. A study of spermatogenesis in the snail *viviparus*. J. Biochem. Biophys. Cytol. 10: 163-193

Gibbons, I.R. and Grimstone, A.V. (1960) On flagellar structure in certain flagellates. J. Biophys. Biochem. Cytol. 7:697-715

Goldstein, P. (1977). Spermatogenesis and spermiogenesis in *Ascaris lumbricoides var. suum*. J. Morph. 154:317-338

Grimes, G.W. (1973). Origin and development of kinetosomes in *oxytricha fallax*. J. Cell Sci. 13:43-53

Kalnins, V.I. and Porter, K.R. (1969) Centriole replication during ciliogenesis in the chick tracheal epithelium. Z. Zellforsch. 100:1-30

Komatsu, M. and Fujita, H. (1978) Electron-microscopic studies on the development and aging of the oviduct epithelium of mice. Anat. Embryol. 152:243-259

Manton, I., Kowallik, K. and von Stosch, H.A. (1970). Observations on the fine structure and development of the spindle at mitosis and meiosis in a marine centric diatom (*Lithodesmium undulatum*). IV. The second meiotic division and conclusion. J.Cell Sci. 7:407-443

Moser, J.W.and Kreitner, G.L. (1970) Centrosome structure in *anthoceros laevis* and *marchantia polymorpha*. J. Cell Biol. 44:454-458

Perkins, F.O. (1970) Formation of centriole and centriole-like structure during meiosis and mitosis in *labyrinthula (Rhizopodea labyrinthulida)* J.Cell Sci. 6:629-653

Phillips, D.M. (1966) Observations on the spermiogenesis in the fungus gnat *sciara coprophilia*. J. Cell Biol. 30:477-497

Phillips, D.M. (1974). In "Cilia and Flagella." (ed. Sleigh, M.A.) Academic Press, London. pp 379-402

Pickett-Heaps, J. (1973) The autonomy of the centriole: Fact or fallacy? Cytobios. 3:205-214

Porter, K.R. (1965) The submicroscopic morphology of protoplasm. The Harvey lectures 51:175-228

Prensier, G., Vivier, E. ,Goldstein, S. and Schrevel, J. (1980). Motile flagellum with a "3+0" ultrastructure. Science 207:1493-1499

Shay, J.W. (1974). Ultrastructural observations on spermiogenesis in the fungus gnat *Rhynchosciara Sp.* In "The Functional Anatomy of the Spermatozoon" (ed. B.A. Afzelius) Pergamon Press, Oxford and New York.

Sorokin, S. (1962) Centrioles and the formation of rudimentary cilia by fibroblasts and smooth muscle cells. J. Cell Biol. 15:363-377

Tamm, S. and Tamm, S.L. (1980). Origin and development offree kinetosomes in the flagellates *Deltatrichonympha* and *Koruga*. J. Cell Sci. 42:189-205.

Turner, F.R. (1968) An ultrastructural study of plant spermatogenesis. J. Cell Biol. 37:370-393.

Vorobiev, I.A. and Chentsov, Y.S. (1982). Centrioles in the cell cycle. I. Epithelial cells. J.Cell Biol.93:938-949.

Wheatley, D.N. (1966) Cilia in cell-cultured fibroblasts. I. On their occurrence and relative frequencies in primary cultures and established cell lines. J. Anat. 105:351-362

FIGURE LEGENDS.

Figure 1.

Simplified schematic of the microtubular skeleton of centrioles and basal bodies.

Figure 2.

The formation of centrioles of 3T3 cells in cross-section. Each column of panels represents a series of sections through a centriole with the distal end at the top panel. The white bar in the top panel of column a indicates 0.2 μm.

a. Pro-centriole. The top panel illustrates a fibrous coil surrounding the beginning blade structures. The arrow in the middle panel points to one of the blades whose C-tubule is still missing. The arrow in the bottom panel points to one of the vesicles surrounding the forming structure.

b-d. Centrioles in increasingly mature stages. The arrows in column b point to the central hub of the proximally located cartwheel which is disassembled in mature centrioles (cf. column d). The arrows in columns c and d point to dense plaques that are attached to some but not all blades.

e. Final stage of many centrioles is the formation of a primary cilium, characterized by the absence of a central microtubular doublet (top panel).

Figure 3

Formation of the centrioles of 3T3 cells in longitudinal section. Bars in panels d and g indicate 0.2 μm.

a-c. Growth of a pro-centriole orthogonally to the wall of a mother centriole seen at the bottom half of each panel.

d-f. Further maturation of the centriole.

g. Primary cilium.

Figure 4

Earliest stages of the formation of a centriole according to the model (Bud-formation).

a. Initial closed ring of 9 microtubular precursors indicated by dotted rings of 1 microtubular diameter. One of the future arms is indicated as a polygon.

b. Addition of 9 further precursors in the densest possible packing.

c. Addition of 9 further microtubular precursors in the densest possible packing. As indicated by the cross-hatched structure, the curved shape of the future triplet blades arises automatically.

d. Separate drawing of one of the 9 arms and its hinge ('*').

e. Three stages of the postulated swivelling of one of the arms around its hinge.

Figure 5

Derivation of the blade curvature. Each dot represents a microtubular protofilament,

a. Illustration of the two theoretical possibilities to attach two C-shaped microtubules (Centers marked B, C and C') to a complete one (center marked A) which are compatible with the postulate of densest packing. The model assumes that protofilaments 1 and 1' or 2 and 2' have to be shared. As a result two blade curvatures $cu=\tau=360^{o}/26=13.85^{o}$ and $cu=3\tau=41.5^{o}$ arise.

b. The resulting bud structure if $cu=3\tau$

c. The resulting bud structure if $cu=\tau$.

Figure 6

Unfolding of the bud by swivelling of each rigid arm around its hinge (Maturation). One of the blades is cross-hatched to illustrate its swivelling. Arrow in panel h points to the reforming ring that has the essential structure of the inital bud.

a-j. Consecutive stages of the unfolding. The blade curvature is $cu=3\tau=41.5^{o}$. The fixed blade angle is 70^{o}. The swivel angles ϕ are a:0^{o}; b:30^{o}, c:60^{o}; d:90^{o}; e:120^{o}; f:150^{o}; g:180^{o}; h:210^{o}; i:240^{o}; j:250^{o}.

k. Mechanical model to illustrate the requirement of connectors ('co' in the right hand panel) which prevent that the arms get entangled during the unfolding. One of the blades is highlighted (arrow) to illustrate the swivelling movement

Figure 7

Schematic drawing of the location of the connectors C_o.

Figure 8

Stereo pair to illustrate the slight downward spiralling of the arms which is necessary to guarantee that the swivelling arms clear each others space (The image for the right eye is on the right- hand side).

Figure 9

Elongation of the blade microtubules in the order A, B and C during the unfolding shown schematically in the panels a. (beginning growth of the A-tubule), b. (continued growth of the A-tubule and the beginning growth of the B-tubule) and c. (Continued growth of the A- and B-tubule and beginning growth of the C-tubule)

Figure 10

Origin of pitch, taper and changing slant of the blades by a lag of swivelling between the distal and proximal end. In the example the swivel angle at the distal end (top) is $\phi_{dist}=220^{o}$ and at the proximal side $\phi_{prox}=145^{o}$. As a result each blade is pitched. Since the diameter of the forming centriole decreases after passing through a maximum (cf Fig. 6g), the diameter at the distal end becomes smaller than at the proximal end thus generating the taper of the centriole. In addition, the slant of the blades turns more tangential after passing the maximal diameter (cf. Fig. 6). Consequently, the slant of the blades at the distal end is more tangential than at the proximal end similar to actual centrioles.

Figure 11

Illustration of the parameters used in equations 1 - 12 (see text.).

Figure 12

Computed relationships between the swivel angle ϕ and several characteristic quatities of the model during unfolding according to equations 2 - 5. In panels a,c,and e the blade curvature was kept constant at $cu=3\tau=41.53^{o}$ while the fixed arm angle was varied (1:nbl=50^{o}; 2:nbl=70^{o}; 3:nbl=90^{o}). In panels b,d, and f the fixed arm angle was kept constant at $nbl=70^{o}$ while the blade curvature was varied (1:cu=13.8^{o} ; 2:cu=41.5^{o}).

a,b: Change of the blade angle bl as a function of the swivel angle.

c,d: Change of the inner radius R_i (radius of the lumen) and outer radius R_o as functions of the swivel angle.

e,f: Change of the inner radius R_i as a function of the outer radius R_o. Arrows indicate the direction of change during unfolding of the bud.

Figure 13

Example of the fitting of actual centriolar cross-sections to the model.

distal

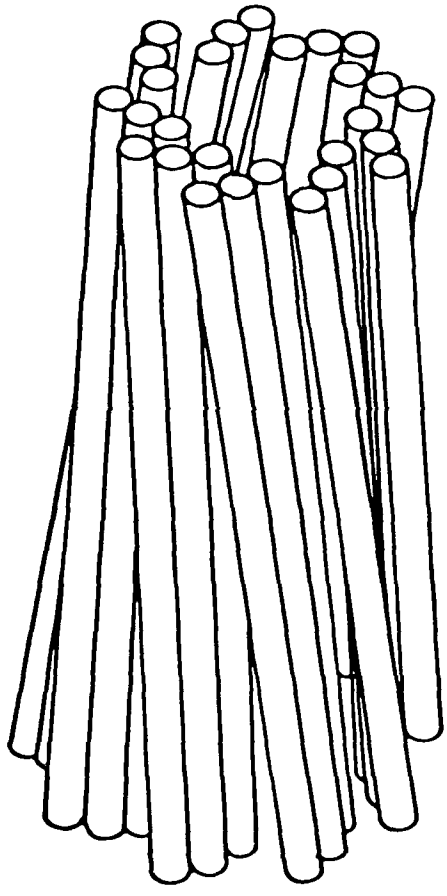

proximal

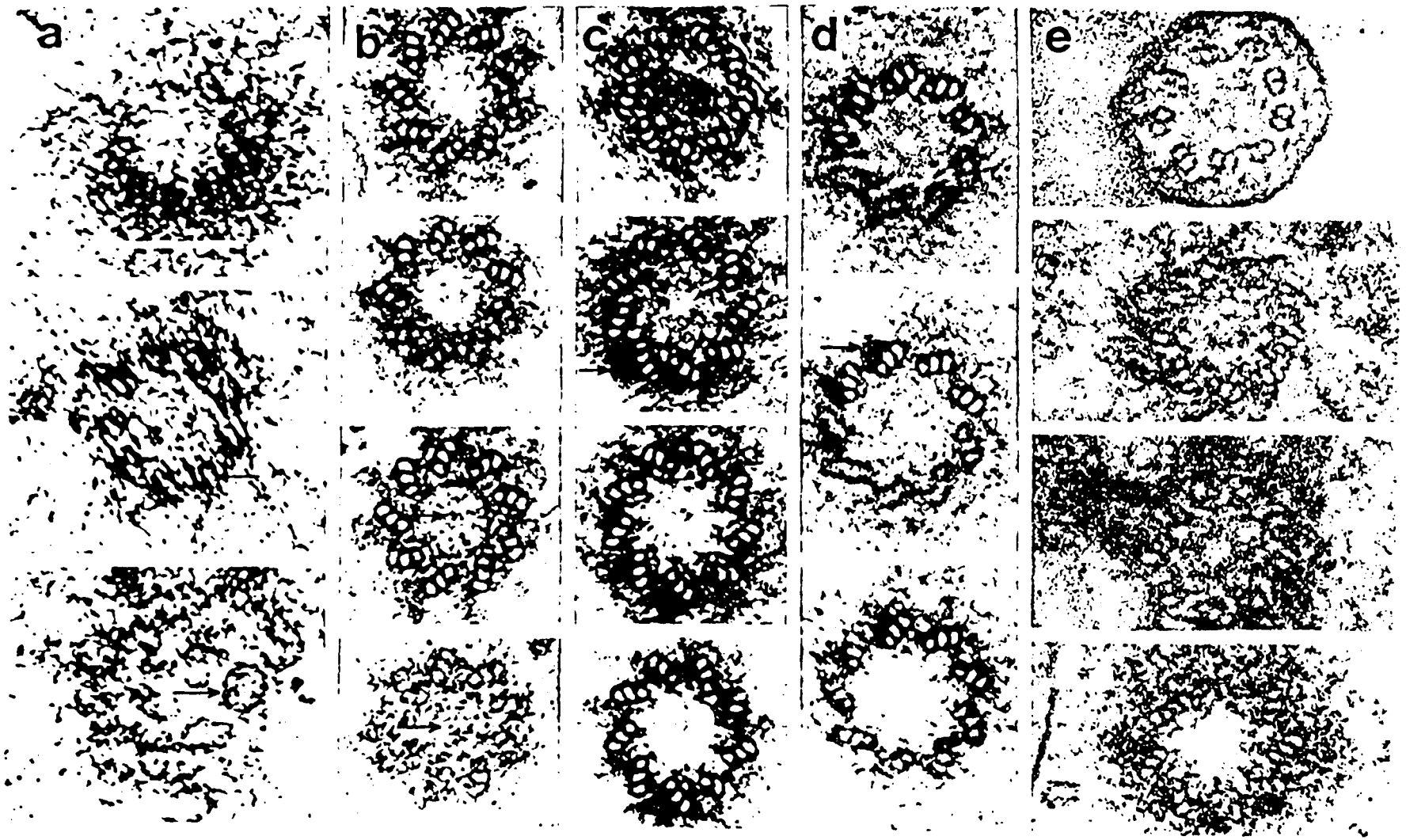
a
b
c
d
e

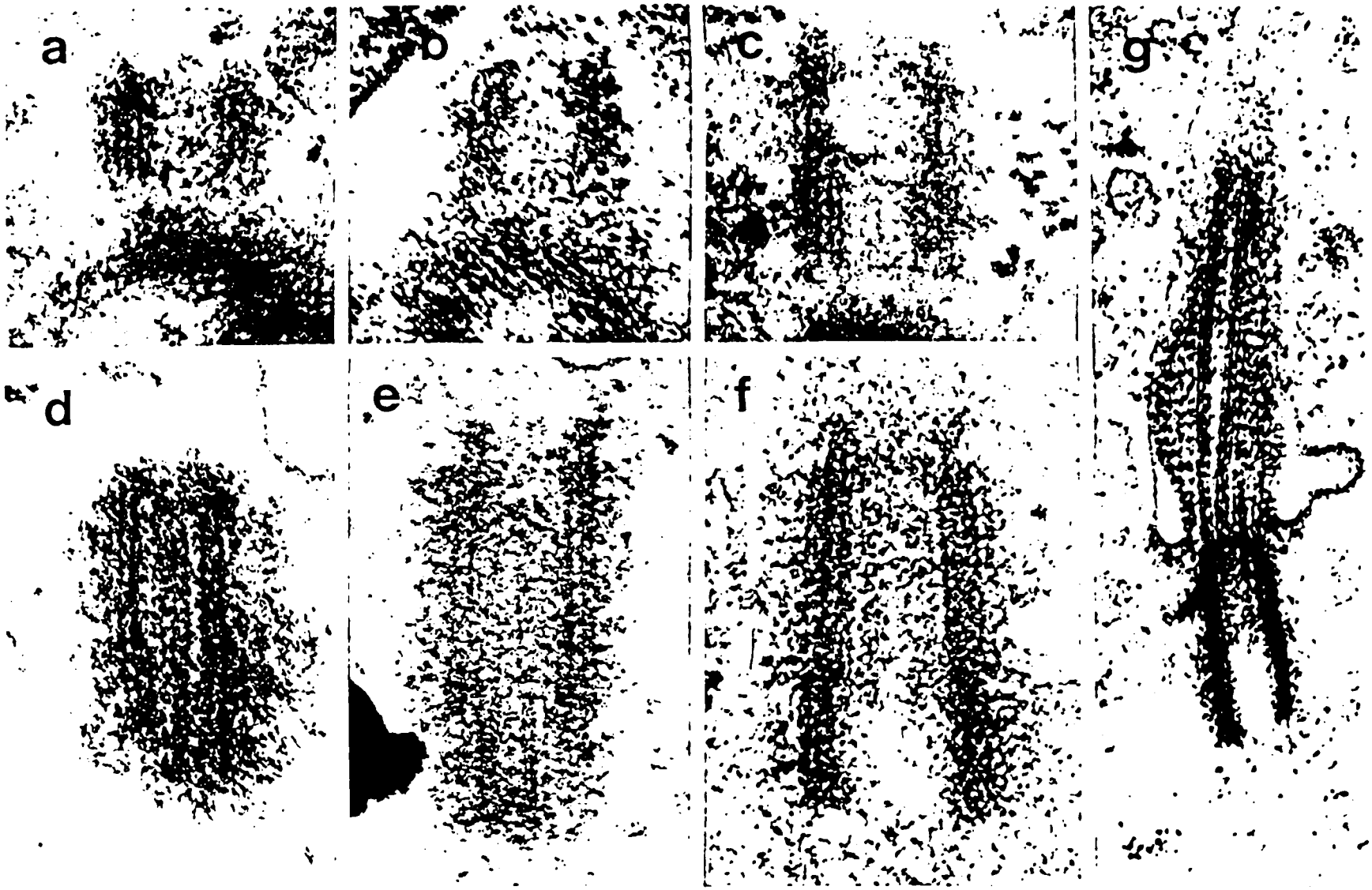
a
b
c
g
d
e
f

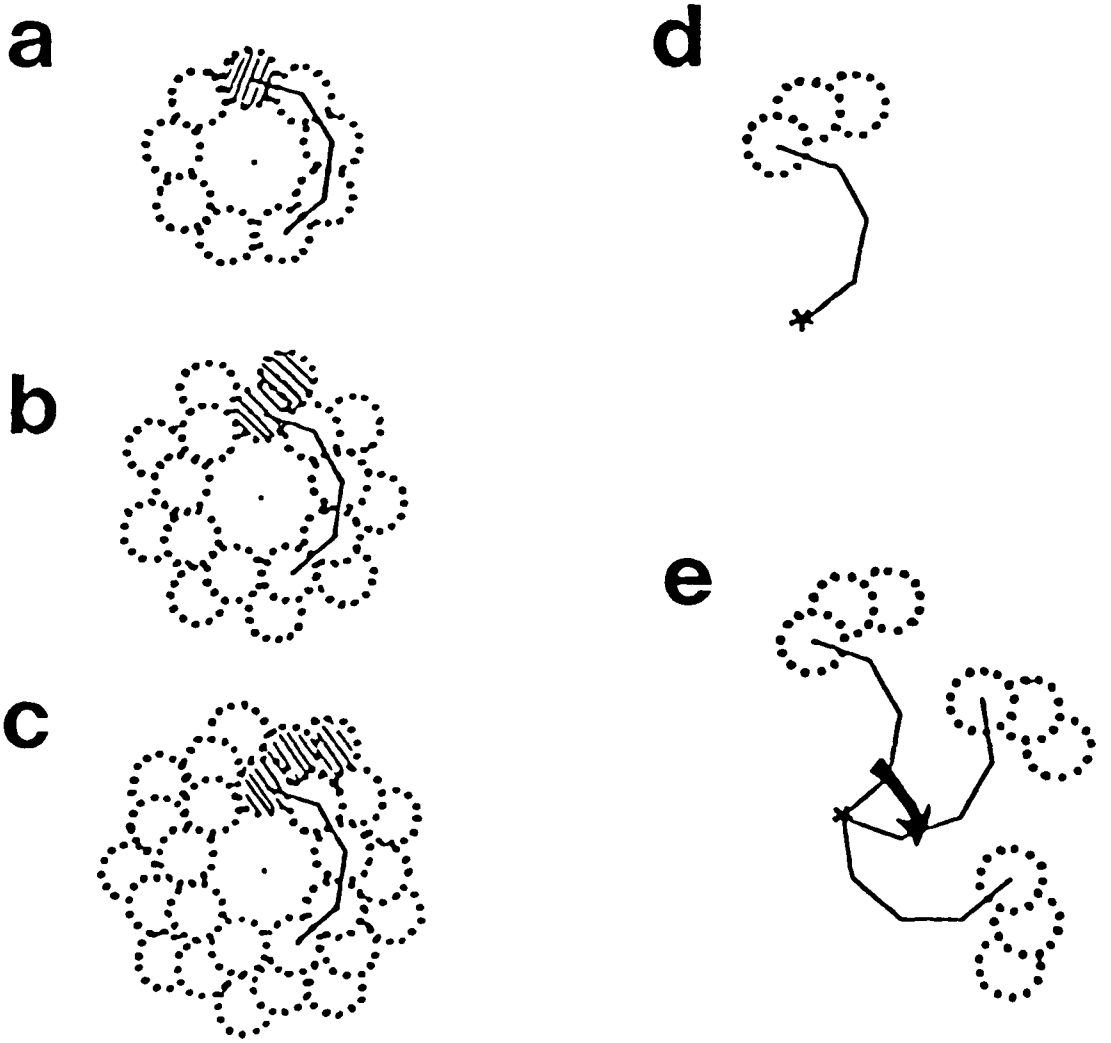
a
b
c
d
e

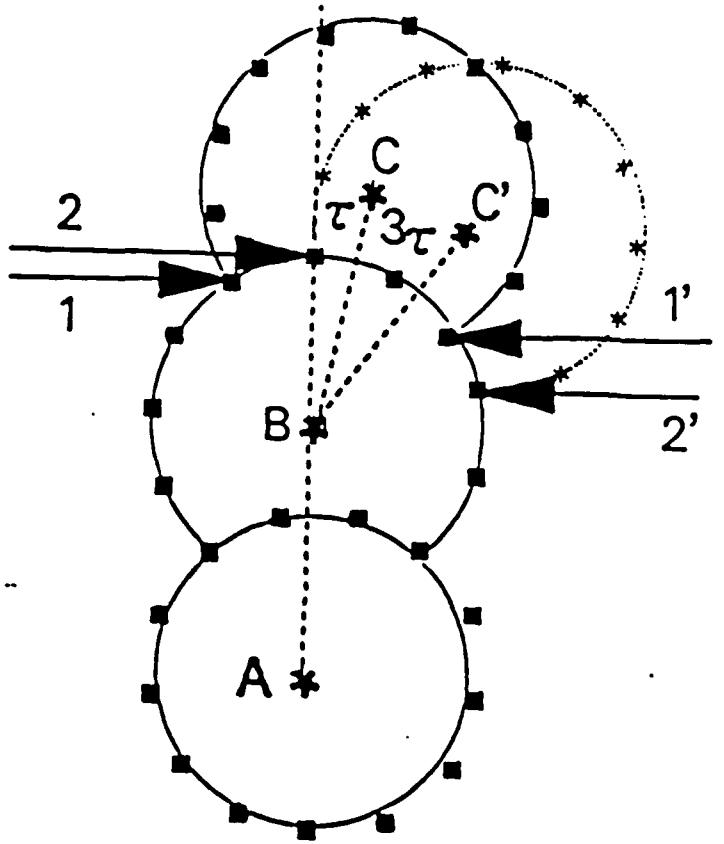

a

b

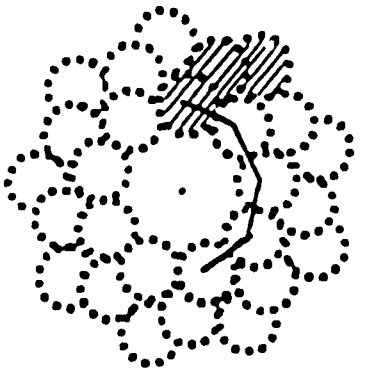

c

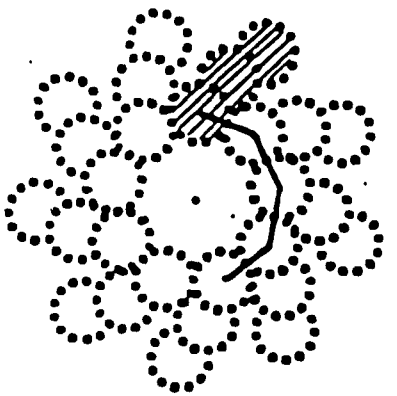

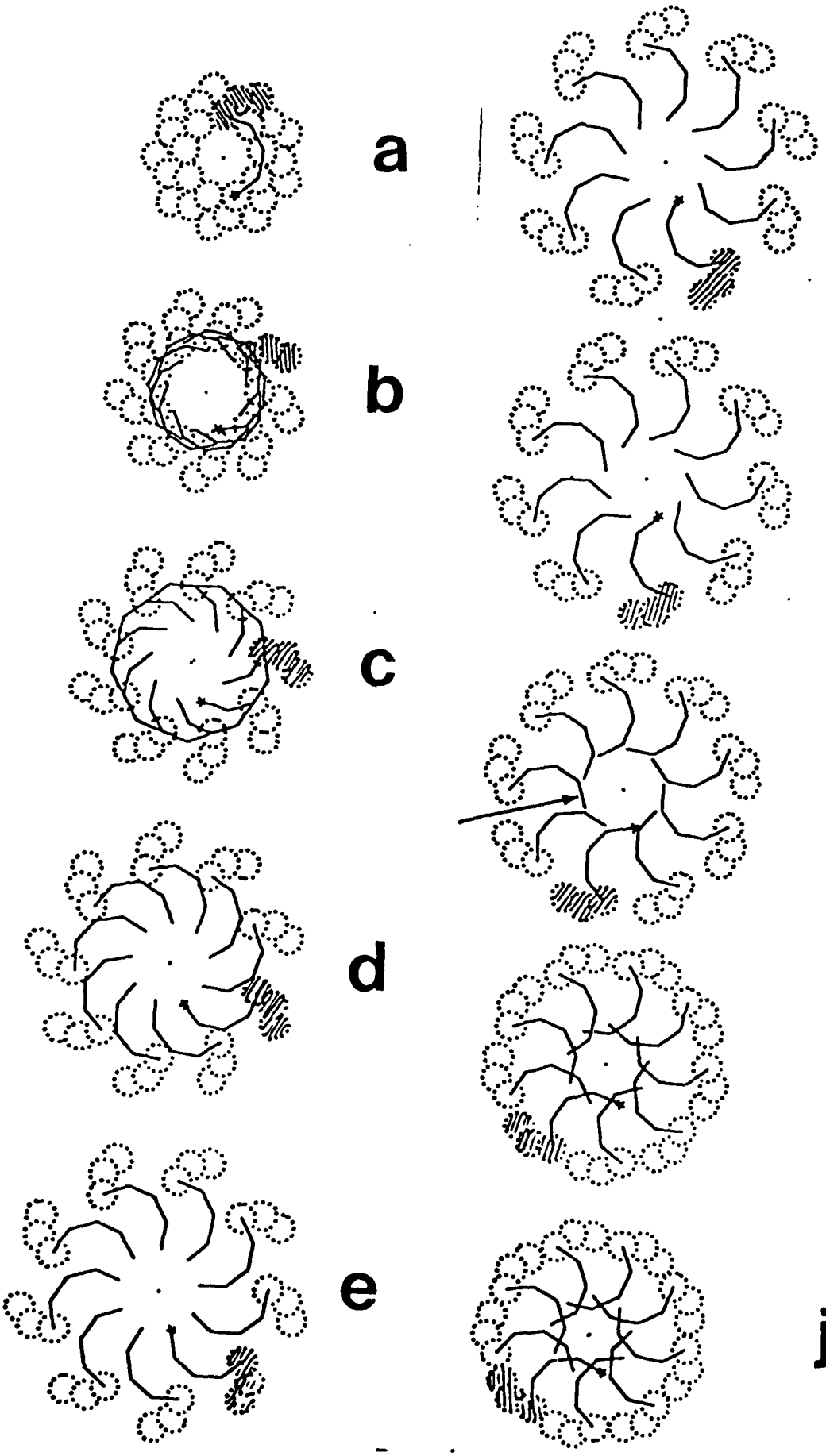
a
b
c
d
e
f
g
h
i
j

120°
0°
15°
90°
0°
50°

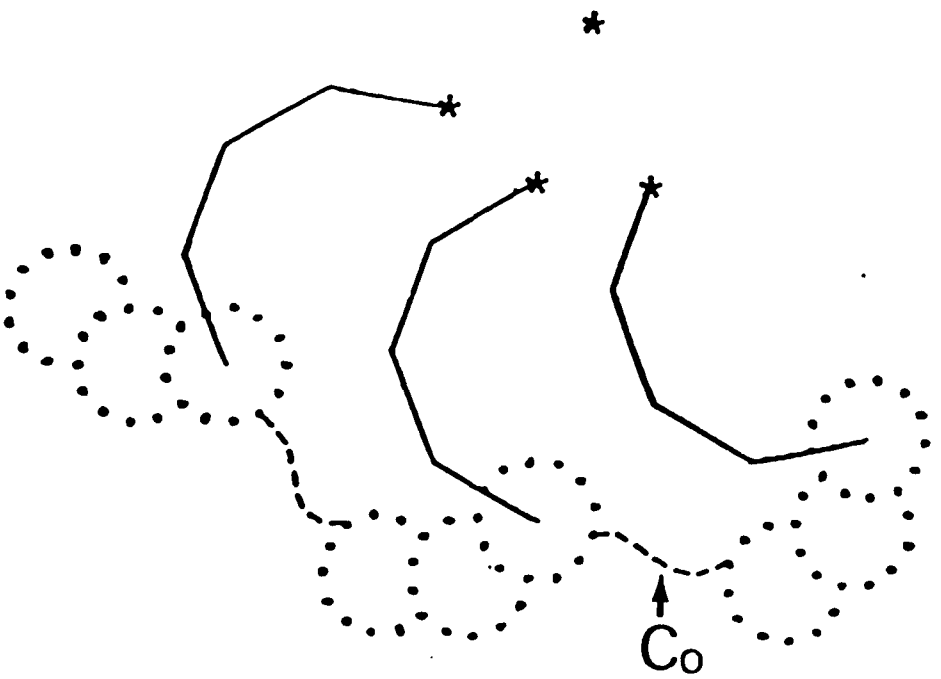
C_o

8

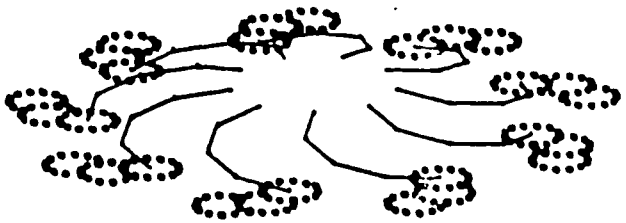

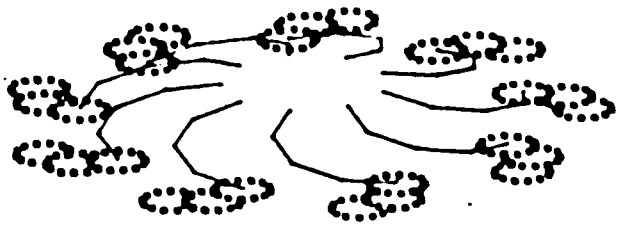

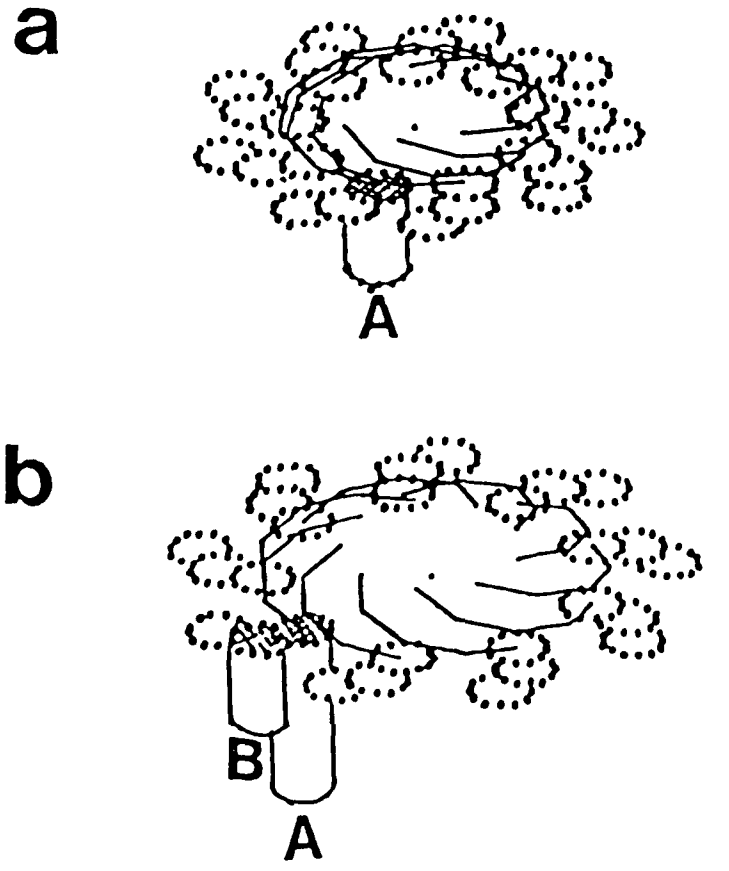
a
A
b
B
A
c
C
B
A

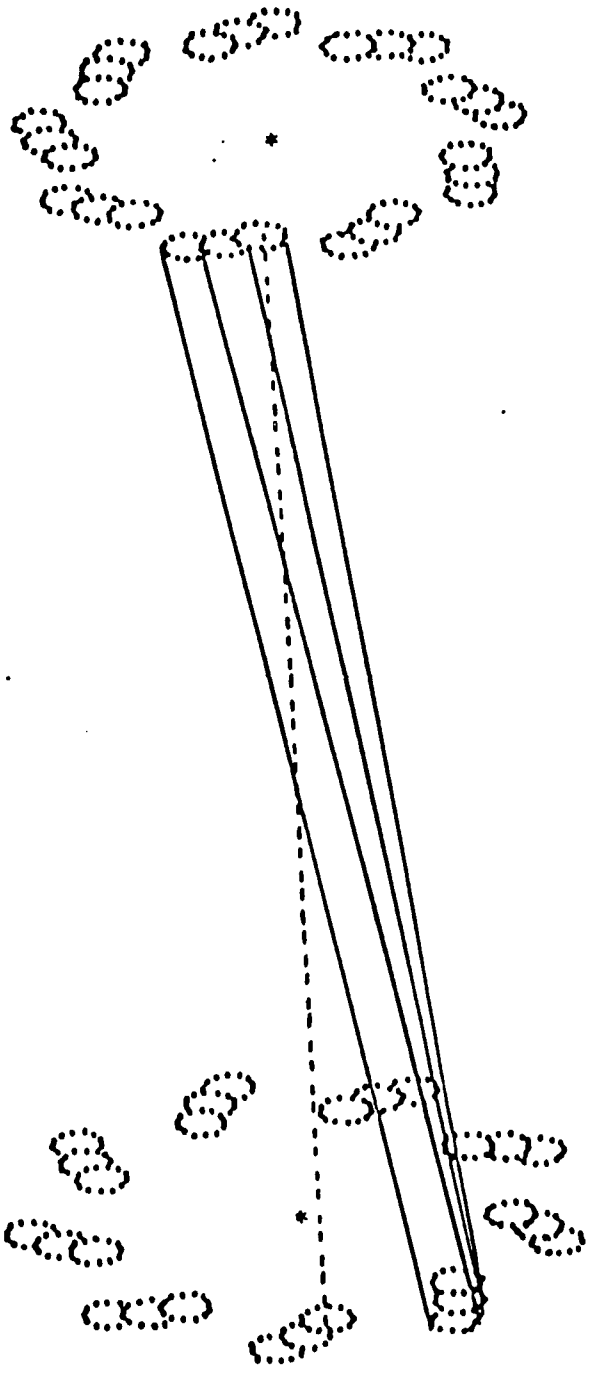

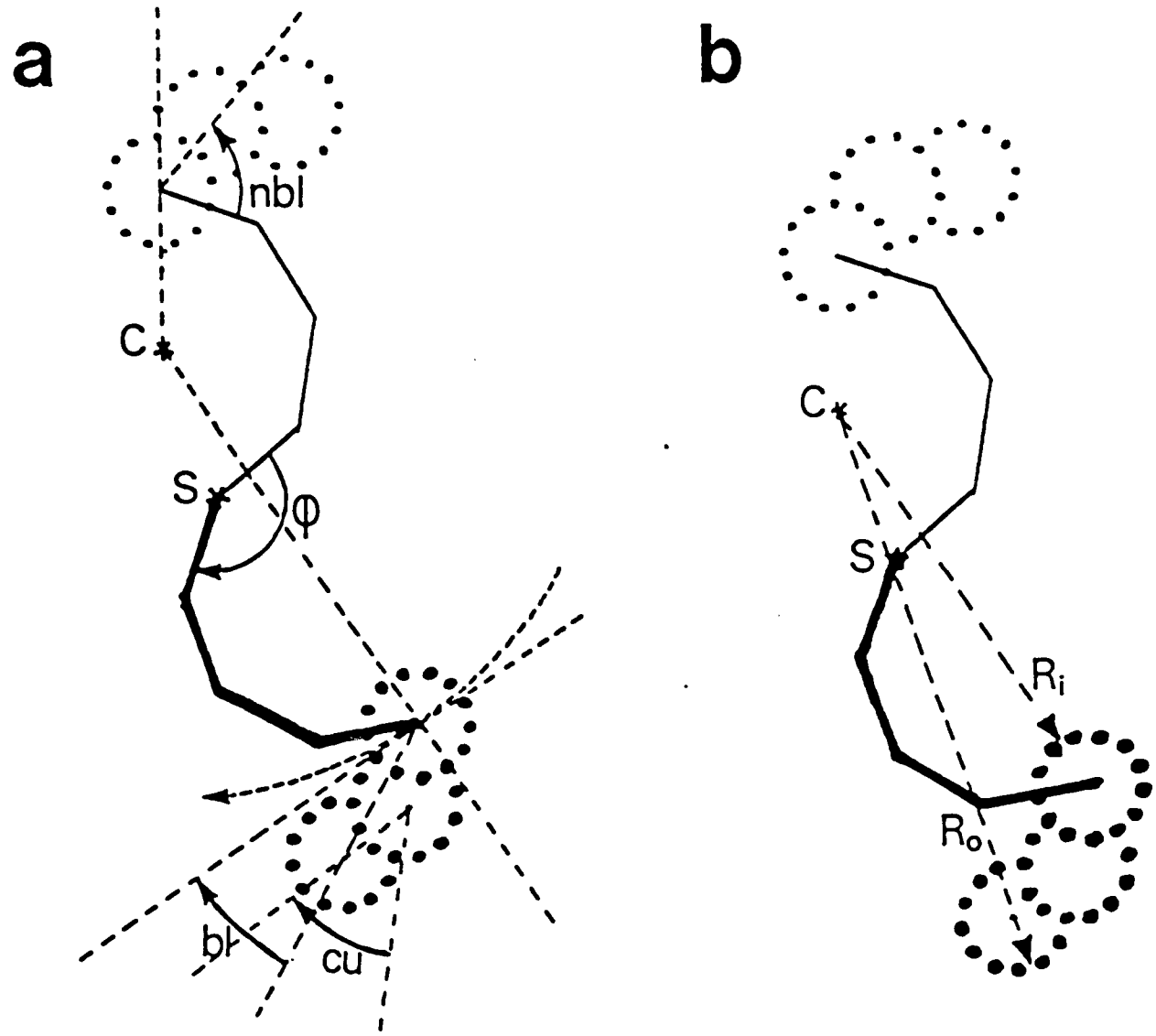
a
nbl
C
S
φ
bk
cu
b
C
S
R_i
R_o

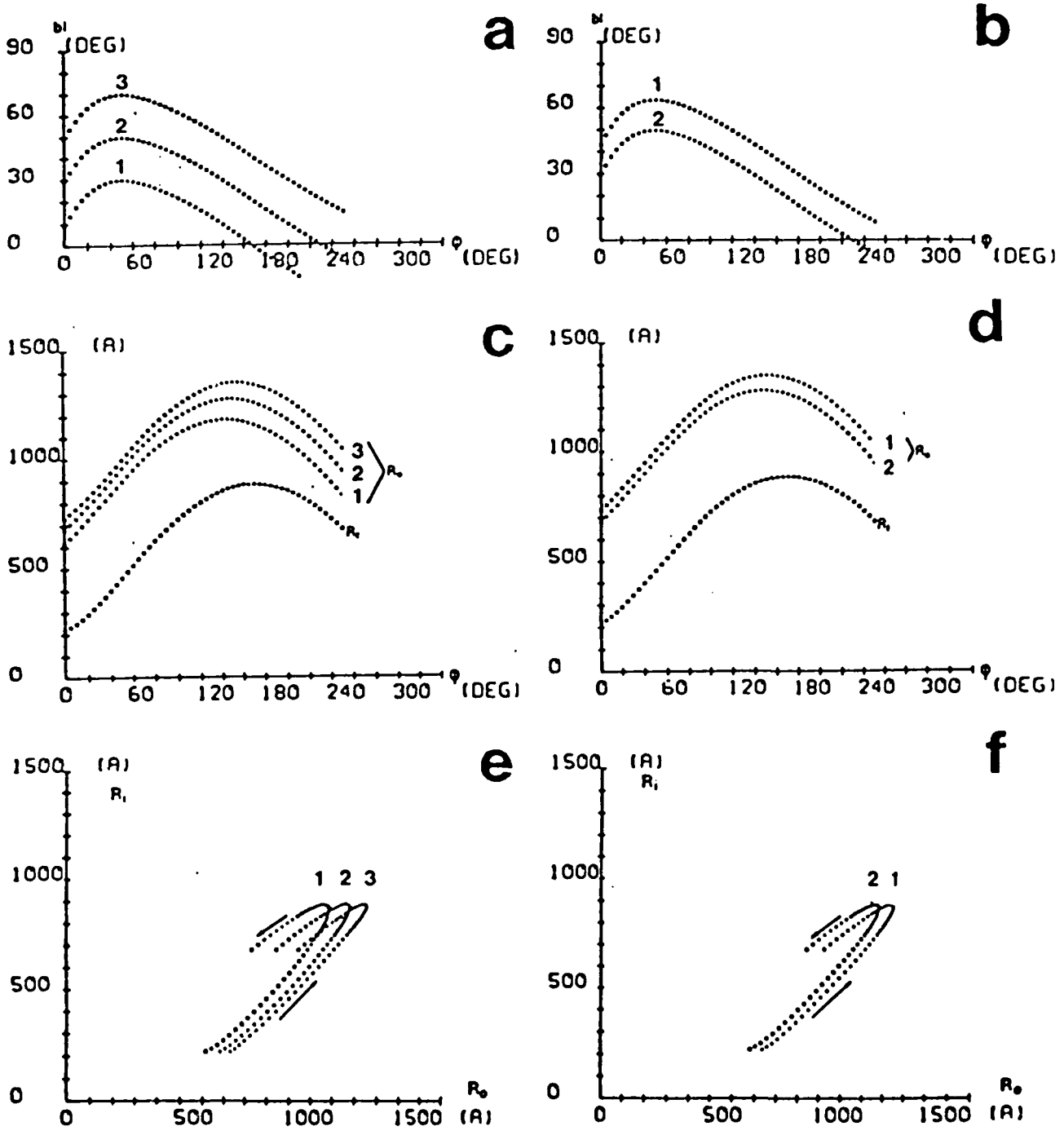
a
b
c
d
e
f
90
60
30
0
(DEG)
3
2
1
0 60 120 180 240 300 φ (DEG)
1500
1000
500
(A)
R_o
R_i
1 2 3
2 1
0 500 1000 1500 (A)

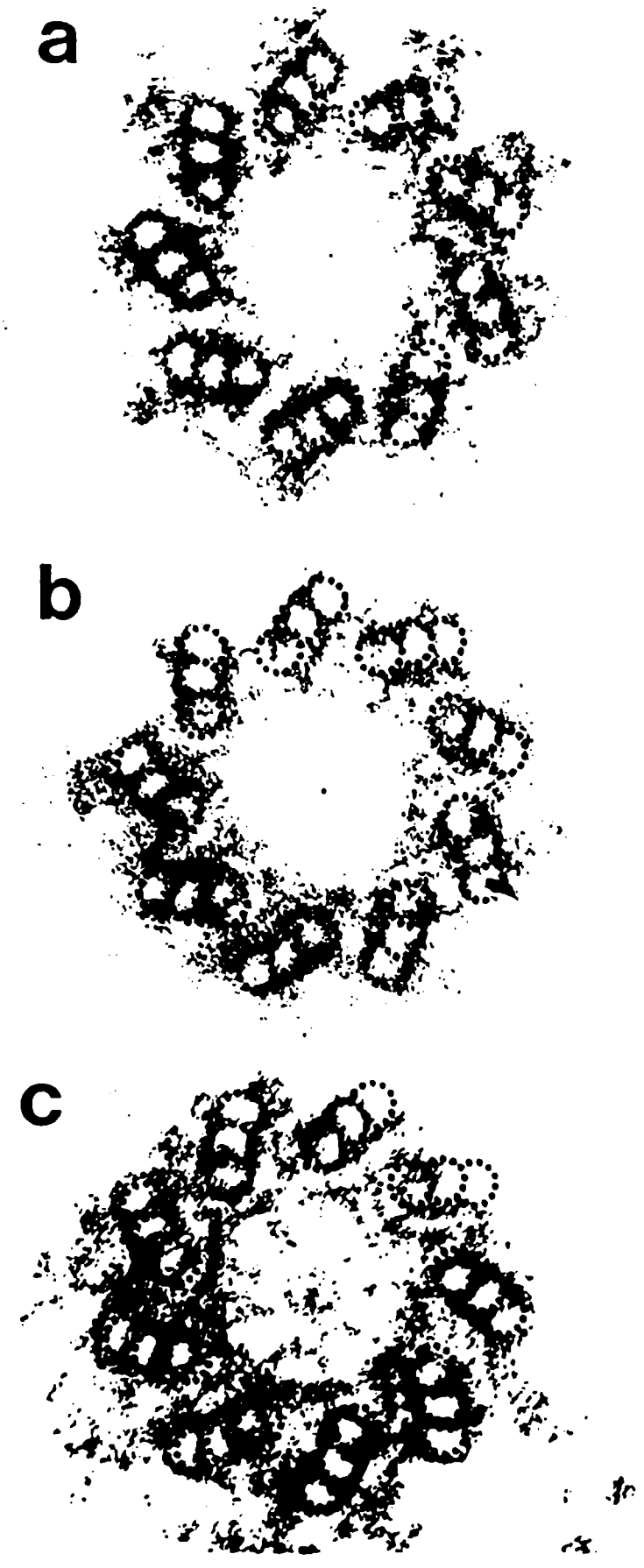
a
b
c